Scientific Reports

https://doi.org/10.1038/s41598-025-28796-8

Article in Press

Revealing vortex structure with pyrocystis lunula bioluminescence

Received: 30 July 2025

Accepted: 12 November 2025

Published online: 27 November 2025

Cite this article as: Castellani L., Ravazzani G., Passoni G. *et al.* Revealing vortex structure with pyrocystis lunula bioluminescence. *Sci Rep* (2025). https://doi.org/10.1038/s41598-025-28796-8

Lucia Castellani, Giovanni Ravazzani, Giuseppe Passoni, Stefano Gomarasca, Ingrid Maria Paoletti & Marco Mancini

Revealing vortex structure with pyrocystis lunula bioluminescence

Lucia Castellani[1,*], Giovanni Ravazzani[1], Giuseppe Passoni[2], Stefano Gomarasca[3], Ingrid Maria Paoletti[4] and Marco Mancini[1]

[1]Politecnico di Milano, Department of Civil and Environmental Engineering (DICA), Milan, 20133, Italy
[2]Politecnico di Milano, Dipartimento di Elettronica, Informazione e Bioingegneria (DEIB), Milan, 20133, Italy
[3]University of Milan, Department of Environmental Science and Policy, Milan, 20133, Italy
[4]Politecnico di Milano, Department of Architecture, Built environment, and Construction engineering (DABC), Milan, 20133, Italy
[*]lucia.castellani@polimi.it

ABSTRACT

The study presented herein examines the vortex structures generated by a magnetic stirrer inside a container filled with seawater and the dinoflagellate *Pyrocystis lunula*. This bioluminescent organism can emit light when water is stirred, due to a natural chemical reaction. The relationship between dinoflagellate bioluminescence and hydrodynamic flow fields has been recently investigated, particularly focusing on water induced shear stress. In the present study, the funnel depth of vortices observed in water stirred experiments are compared with existing vortex models, and the shear stress distribution within the flow field is estimated. The results indicate that, for the range of angular velocities analysed and the geometry of the experimental setup, *Pyrocystis lunula* bioluminescence can serve as an indicator of the vortex structure. Furthermore, this study confirms the validity of *Pyrocystis lunula* as a biological sensor of tangential shear stress in fluid domains, specifically within vortical flows. The dinoflagellate species may serve as a low-cost tool to visualize fluid structures in hydrodynamic experiments in which the flow field must remain undisturbed by external instrumentation. Additionally, the study suggests a potential approach to designing applications with dinoflagellates: by enabling the formation of controlled light patterns, hydrodynamics may serve as a functional design parameter.

Keywords: Bioluminescence, Pyrocystis lunula, Rankine vortex, Shear stress, Flow tracer, Water stirrer, Biosensor

Introduction

Bioluminescence consists in the light emission by some living organisms. It is linked to specific taxonomic groups - genera and species - and can present multiple colors, colors that are closely linked to the individual taxonomic group. This phenomenon is the result of a chemiluminescent reaction catalyzed by an enzyme called luciferase. During this reaction, luciferin is oxidized, forming oxyluciferin in its excited state. In the subsequent decay to the ground state, photons are emitted as visible light[1]. Bioluminescence predominantly occurs in marine environment[2], and represents a significant Earth ecological trait[3]. Bioluminescent dinoflagellates are widespread microorganisms that live on sea surface[2]: the light trigger represents a defensive strategy, e.g. making their predator more vulnerable to other predators[4].
Several studies have shown that bioluminescence in dinoflagellates is triggered by mechanical stresses generated by the fluid flow; most of these investigated the shear

stress threshold required to activate bioluminescence, focusing on fully developed pipe flow and simple Couette flow[5–9]. Latz et al. (1994)[5] showed that in simple Couette flow the light intensity increases proportionally to the applied stress, and that dinoflagellate bioluminescence is triggered also in laminar regime, without requiring the presence of turbulence. Rohr et al. (1997)[6] confirmed the independence of bioluminescence from flow regime, showing that the light intensity of *Lingulodinium polyedrum* remained essentially invariant under both laminar and turbulent conditions in fully developed pipe flow. For this species, the shear stress activation threshold was estimated to be approximately 0.3 N/m^2 [7]. Latz et al. (2004)[8] further investigated the bioluminescent response of four dinoflagellate species in fully developed pipe flow, analysing both average and peak light intensities, and proposing a relationship linking mean bioluminescent intensity to shear stress and organism concentration in the fluid. The dependence of bioluminescence on shear stress was confirmed by Maldonado and Latz (2007)[9], who altered fluid viscosity and observed that, under a steady laminar shear stress applied in a simple Couette flow, the intensity of bioluminescence was greater in the fluid with increased viscosity.

Bioluminescence can be used in laboratory as an incomparable indicator of the flow field, as far as it represents a passive flow tracer that can be seen when hydrodynamic stimuli overcome a threshold level[10]; furthermore, dinoflagellates allow flow visualization at cell concentrations that do not alter fluid viscosity, preserving its Newtonian behavior[11]. Consequently, the study of bioluminescent emission finds practical application in flow visualization techniques[12]. The shear stress threshold required for bioluminescence triggering can be used to quickly assess the flow conditions within a system[13], enabling the use of dinoflagellate as a quantitative tool to investigate complex flow fields difficult to analyze[8]. Deane et al. (2016)[14] examined the shear stress induced by single rising bubbles and bubble plumes, establishing a correlation between bubble radius and the resulting shear stress, in order to predict cell stimulation in *Lingulodinium polyedrum*. Blaser et al. (2002)[15] investigated dinoflagellate bioluminescence under various hydraulic conditions, including the turbulent flow field generated by a stirring device. Their experimental setup employed a relatively small volume (50 mL) and focused on quantifying maximum and mean light intensity as a function of rotational speed, as well as analyzing bioluminescence decay over time. Marking out cell stimulation, such prediction can also be an effective tool in designing and optimization of bioreactors[16]. Chen et al. (2002)[16] employed the bioluminescence of *Pyrocystis fusiformis* to evaluate different impellers in agitated bioreactors, aiming at identifying the design that minimized cellular stimulation.

As far as we are aware, the use of dinoflagellates as visualizers of vortex structures generated by a magnetic stirrer inside a container has not been previously reported. Although Chen et al. (2002)[16] observed bioluminescence at the free surface of the vortex above certain agitation speed thresholds, it was not included in the main analysis of the work. Einstein (1926)[17] was the first to provide a physical explanation of the secondary vortical motions that develop inside a container, using the example of a tea cup stirred with a spoon to illustrate the origin of meander formation in river channels. Halasz et al. (2007)[18] investigated the swirling flow generated by a magnetic stirrer with different geometries of cylindrical containers and stirrer bars, pointing out that the geometry of the vortex can be predicted based on the known stirrer bar and the cylindrical container geometries, combined with the angular velocity and fluid properties. However, the equations governing vortical motion are quite complex; therefore, the use of simplified analytical models, such as the Rankine (1858)[19] combined vortex, is justified[20]. According to this model, a free and a forced vortex coexist, each governed by its respective tangential velocity profile, separated by a cylindrical surface[19] whose radius is referred to as the core radius[21].

The aim of the present study is to evaluate the potential of dinoflagellate *Pyrocystis lunula* bioluminescence as a biological visualizer of shear stress within vortical flows generated by a magnetic stirrer inside a cylindrical glass container, focusing on the

tangential velocity field and using the Rankine (1858)[19] vortex to characterize it. The objective of the work is to ascertain if *Pyrocystis lunula* bioluminescence can reveal details about the underlying vortex structure, assessing whether light emission patterns correspond to zones of elevated shear stress. It is expected that the regions of highest shear stress along the vortex free surface – particularly near the vortex core – may trigger dinoflagellate bioluminescence, if the shear stress exceeds the activation threshold. For *Pyrocystis lunula*, this threshold is estimated to be approximately 0.2–0.3 N/m^2, as in a previous study by Cussatlegras and Le Gal (2007)[22]. The work is divided into three main phases: firstly, an experimental setup is established to observe the bioluminescence patterns of *Pyrocystis lunula* associated with vortex structures generated at different angular velocities, and the relative pictures are shown in Results as Qualitative images assessment. Then, vortex geometries acquired in the images during the experimental phase are compared with the model proposed by Halasz et al. (2007)[18], to verify the coherence between the experimental geometries and the model. Finally, approximating the case study with a Rankine (1858)[19] vortex, the same geometries are overlapped with the bathtub vortex depth of the central depression as described by Lautrup (2005)[21]. The funnel depth, maximum shear stress and tangential velocity as function of all the angular velocities considered are shown in Results as Quantitative image assessment; the overlapping with the photograph for 160 rad/s is shown, together with tangential velocity and shear stress plots. The shear stresses are compared with literature values known to activate bioluminescence in *Pyrocystis lunula*. Finally, observations are presented regarding the analogy between vortex structures and the observed bioluminescence patterns, suggesting that *Pyrocystis lunula* can be used as a tool to visualize fluid structures, but also that hydrodynamic can be used as a method for design and compose light.

Results

Qualitative images assessment

The photographs in Figure 1 show that the light intensity is concentrated in three main regions: at the base of the glass container where the stirrer bar rotation occurs, at the lowest central point of the funnel-shaped free surface, and approximately halfway up the funnel. The latter feature is the primary focus of this study: specifically, it is observed that at about half the depth of the vortex, a luminous strip is generated, indicating that tangential stresses are higher in this zone. This finding is consistent with the Rankine (1858)[19] vortex and Lautrup (2005)[21] which predict that the maximum tangential stress occurs just before the core boundary.

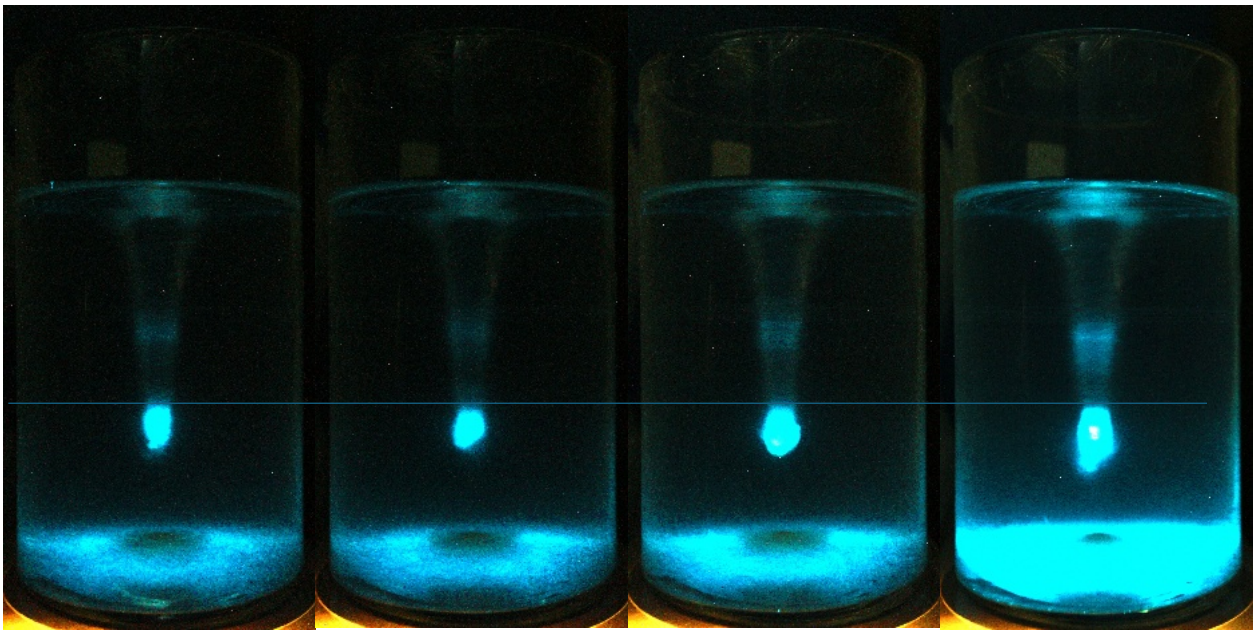

(a) **(b)** **(c)** **(d)**

Figure 1: Pictures of different funnel structures corresponding to different angular velocities, showing a bioluminescent strip at the halfwidth of the vortex: 152 rad/s **(a)**, 154 rad/s **(b)**, 157 rad/s **(c)**, 160 rad/s **(d)**. As angular velocity increases, a corresponding increasing in visible light intensity is observed in the images. The brightness and white balance of the photographs are enhanced to improve the visualization of the bioluminescent regions of the vortex, activated by shear stress.

The fluid at the base of the container and the central tip of the funnel emits the majority of the light intensity, indicating that the highest shear stresses occur in these two regions. While the emission at the base of the container is stationary, the brightness at the vortex tip follows its shape and tends to display irregular patterns downward until the vortex stabilizes. However, the vortex stability is delicate, and even during image acquisition, oscillatory downward motions of the vortex are observed. It is also observed that, as the vortex velocity increases, the depth of the funnel increases, in agreement with models predictions[18,21]. Although the photographs reveal some light emission at the upper free surface of the vortex, this is mainly due to the reflection of light emitted from the bottom. Nonetheless, some luminous filaments are effectively visible in the experiment, suggesting that *Pyrocystis lunula* are also stimulated in the upper region and emit bioluminescence. Overall, the photographs show that *Pyrocystis lunula* may serve as indicators of zones experiencing the highest shear stress within the vortical flow.

Quantitative images assessment

Comparison of the experimental vortex geometries with Halasz et al. (2007)[18] model shows that within the parameter range considered in the reference study, the values that best fit the experimental data are: $\alpha = 620$, $\kappa = 3000$, and $\beta = 2350$. Using these parameters, it is found that for all rotation frequencies, the parameter b equals 0.006 m, while the funnel depth Δh [m] as a function of angular velocity Ω [rad/s] is shown in Figure 2 (a). The value of L [m], determined from the images, is approximately 0.145 m across all tested angular velocities, while circulation values C [m^2/s] are within the range 0.00573 m^2/s – 0.00603 m^2/s. In Figure 2 (a) values of Δh [m] and $(L - h_0)$ [m] are compared with the experimentally measured depths. Both computed parameters are consistent with the observed vortex geometries, and the study reveals an approximately pseudo-linear trend in the experimental depth. The overlapping of

vortex profiles obtained from Lautrup (2005)[21] onto the experimental photographs made it possible to associate the free surface depression with tangential velocity and the tangential velocity-induced shear stress in the radial direction fields of the Rankine (1858)[19] vortex. The plots shown in Figure 2 (b)–(c) indicate that for angular velocities between 152 rad/s and 160 rad/s, the maximum tangential velocity at the vortex core radius lies within the range of 0.955 m/s to 1.004 m/s, while the corresponding shear stress ranges from -0.343 N/m² to -0.361 N/m².

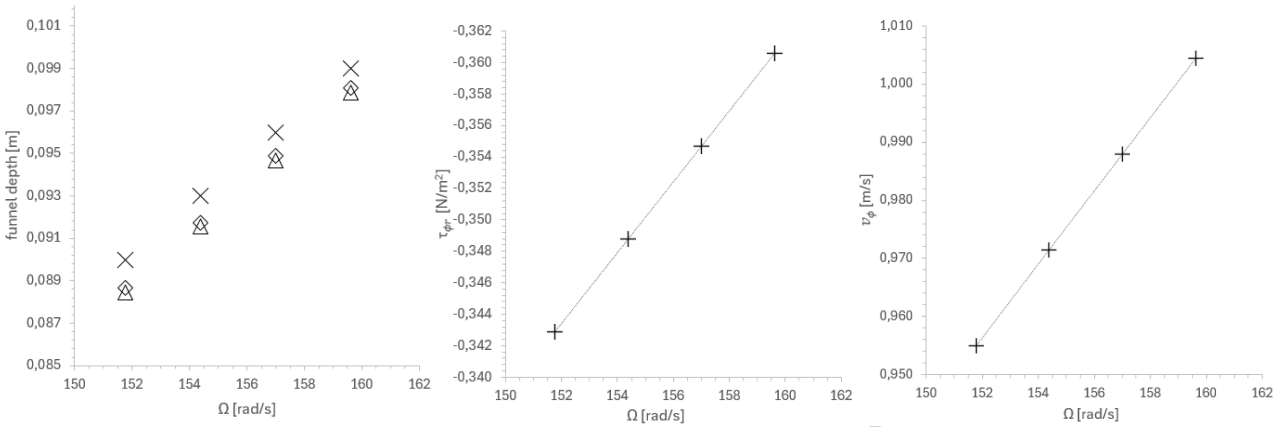

Figure 2: **(a)** Increase of the funnel depth [m] as a function of angular velocity [rad/s]. Triangles represent the values of Δh from Halasz et al. (2007)[18], while rhombuses indicate the values of (L − h₀) from Lautrup (2005)[21]. The values marked with a cross correspond to the experimentally observed depths. Both models results are consistent with the measured ones and exhibit a pseudo-linear trend. Maximum shear stress [N/m²] **(b)** and tangential velocity [m/s] **(c)** fields at the vortex core radius as a function of angular velocity [rad/s], according to Rankine (1858)[19] vortex and Lautrup (2005)[21].

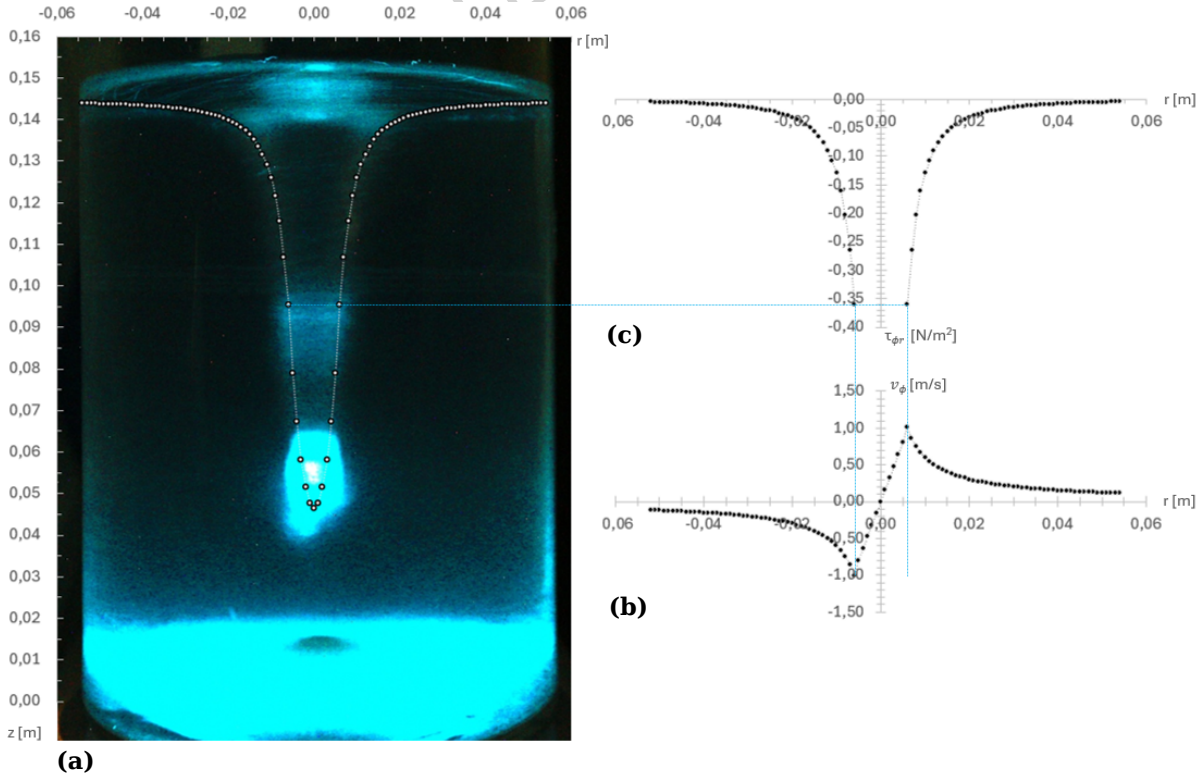

Figure 3: **(a)** Overlapping of bathtub vortex depth of the central depression from Lautrup (2005)[21] with the photograph of the experiment at 160 rad/s. A bioluminescent strip is visible at the half-height of the

funnel. This region corresponds approximately to the core radius height. Values of tangential velocity [m/s] **(b)** and shear stress [N/m^2] **(c)** are shown for each radial position. The maximum value corresponds to the one at the vortex core radius: the brightness and white balance of the photograph are enhanced to improve the visualization of the bioluminescent strip in its proximity.

Figure 3 (a) shows the bathtub vortex depth of the central depression from Lautrup (2005)[21] overlapped on the photograph of the experimental setup at an angular velocity of 160 rad/s. Figure 3 (b)–(c) display the tangential velocity and shear stress profiles as functions of the radial coordinate, according to the Rankine (1858)[19] vortex and Lautrup (2005)[21]. This analysis is carried out for all experimental images acquired under the different angular velocities tested (Figure 1 (a)–(d)). The plots in Figure 2 (a)–(c) confirm that the maximum tangential velocity occurs at the vortex core radius, reaching values of approximately 1 m/s. At the same radial position, the maximum tangential velocity-induced shear stress in the radial direction is also observed, with a value of -0.361 N/m^2. The overlapping of vortex geometries generated at different angular velocities, reveals that bioluminescence is concentrated around the strip at mid-height of the vortex, corresponding to the point where the velocity profile of the the Rankine (1858)[19] vortex changes. This point marks the ideal transition in the governing velocity regime[21], and coincides with the location of maximum shear stress.

Discussion

The bioluminescence patterns concentrated at the base of the container show similarities with the study by Chen et al. (2002)[16], where bioluminescence was observed mainly in the fluid region between the impeller and the bioreactor walls. Similarly to the observations by Blaser et al. (2002)[15], the present study also reports an increase in light intensity with increasing angular velocity. The range of angular velocities was selected to reproduce a stationary vortex and to reach shear stress values close to the predicted bioluminescence activation threshold of *Pyrocystis lunula* reported in the literature, and because increasing the angular velocity resulted in a longer stabilization time and a less well-defined vortex geometry in the photographs. The chosen range also allowed the funnel geometry to be clearly captured within a few minutes of switching on the magnetic stirrer. The measurements are repeatable under controlled conditions; however, a limitation of the study regards biological variability that must be considered. Specifically, bioluminescent intensity tends to gradually decrease with prolonged operation of the magnetic stirrer, likely due to cellular fatigue or adaptation. While the experimental setup is consistent and reproducible, the biological nature of the system imposes certain limitations that must be taken into account, such as the circadian rhythm of the dinoflagellates and the gradual decrease in light intensity with prolonged stimulation.

The model proposed by Halasz et al. (2007)[18] is used to compare the vortex depth and the half-height radius with the experimental results obtained. For each angular velocity considered, three experiments were conducted to identify the flow field and assess its representativeness through bioluminescence. As noted by Halasz et al. (2007)[18], although the system allows for the reproduction of a statistically steady vortex, fluctuations are present due to the absence of a fixed rotation axis, turbulence, and the periodic movement of the stirrer bar. The vortex depth was estimated from the photographs with a certain degree of approximation due to the resolution of the images and because the vortex fluctuations are captured by the long exposure of the photographs. A limitation of the study is that, since the number of experiments was not sufficiently high, the uncertainty was not evaluated as a true estimate of the variance, but rather as the range of variability observed in the measurements of the vortex core radius and the vortex depth. This uncertainty is associated with both the inherent variability of the phenomenon (as the vortex fluctuates) and the interpretation of the

images, which depends on the digitization of the photographs and on the precise definition of the boundary line between the illuminated and non-illuminated regions. In particular, at the lowest central point of the funnel-shaped free surface, an illuminated region can be observed that represents the vertical fluctuation of the vortex, covering a height of approximately 10 mm. For the core radius, a variability of about 1 mm was observed, mainly due to the difficulty in precisely defining the boundary of the vortex structure. This uncertainty also depends on the capabilities of the camera and the image sharpness at high ISO values, where noise limited the achievable accuracy. The image acquisition technology could be improved in future measurements. For each measurement, the uncertainty was estimated to be approximately ±5 millimeters for the vortex depth, and ±1 millimeter for the core radius. These uncertainties are of the same order as the 10% error reported by Halasz et al. (2007)[18]. Even though in this study the geometric relationship is $R<0.4 \cdot H$, the model accurately predicted the experimental results within the reference ranges of α, κ and β. Approximating the case study with a Rankine (1858)[19] vortex, the comparison is also carried out with the bathtub vortex depth of the central depression from Lautrup (2005)[21]. In this case as well, the experimental results are consistent, showing good agreement with the reference models. Although Halasz et al. (2007)[18] indicates greater consistency with the Burgers (1948)[23] vortex— which might more comprehensively describe the flow field generated in a container, where vortex structures are formed by a magnetic stirrer—the results show that the bathtub vortex depth of the central depression from Lautrup (2005)[21] is also a good indicator of free surface lowering in vortex motion induced by a magnetic stirrer. It is therefore assumed that this model can provide a good approximation of the tangential velocity field, combining the free and forced components of the Rankine (1858)[19] vortex. While the study indicates consistency with the models, further investigations would certainly be beneficial to interpret the results by considering other vortex models that also take into account the radial and axial velocity fields. The contribution of the present work is to propose an additional low-cost method to visualize the regions where shear stress is concentrated in vortices generated by a magnetic stirrer. From a quantitative perspective, the study enables the identification of areas where shear stress exceeds the activation threshold for *Pyrocystis lunula* bioluminescence.

Shear stress values in proximity of the vortex core radius of are consistent with *Pyrocystis lunula* bioluminescence activation threshold, estimated to be around 0.2–0.3 N/m^2 in a previous study by Cussatlegras and Le Gal (2007)[22]. Herein, within the angular velocities considered, this threshold is exceeded in proximity of the vortex core radius, while lower shear stress values are observed at larger radial distances ($r > c$). This threshold is confirmed by the bioluminescent strip observed in proximity of the core radius, demonstrating the consistency of the Rankine (1858)[19] vortex model and Lautrup (2005)[21] in interpreting the tangential velocity field. It is therefore seen that, for the analysed angular velocity ranges and in agreement with the geometries of the experimental setup, *Pyrocystis lunula* can serve as an indicator of the vortex core radius and the ideal transition point between the two governing equations of the Rankine (1858)[19] vortex. However, the present study is limited to a specific angular velocity range and experimental setup geometry; further investigations are needed to confirm this hypothesis under other conditions. Lautrup (2005)[21] indicates that the maximum shear stress occurs just before the vortex core radius and predicts non-zero shear stress only for $r>c$. In this study, shear stress is evaluated up to $r=c$, where the maximum value is reached; however, the images reveal bioluminescence activation even within the vortex core, i.e., for $r<c$. This may be due to the accumulation of *Pyrocystis lunula* at the free surface of the vortex for $r<c$. A similar behaviour was observed when injecting dye inside the core radius and the dye remains confined[18,24].

The prediction of the bioluminescent pattern corresponding to the vortex core has been confirmed by experimental observations. Pictures analyzed were referred to 30 seconds of exposure time of the camera, taken when the vortex structure was quite

clear. Further investigations are needed to determine whether bioluminescence can be employed to explore vortex formation dynamics and their evolution.

Conclusion

This study highlights the suitability of *Pyrocystis lunula* as an indicator of vortical flow and supports the validity of tangential velocity field of the Rankine (1858)[19] vortex and Lautrup (2005)[21]. In particular, the present study shows how *Pyrocystis lunula* bioluminescence can reveal the main details about the underlying vortex structure and the regions of highest shear stress along the vortex free surface. The dinoflagellate response could be a biological sensor for shear stress within a fluid domain, for stresses that exceed the threshold of 0.3 N/m^2, approximately. This finding supports a non-invasive and low-cost technique to investigate hydrodynamic behaviour without disturbing the flow field, suggesting that *Pyrocystis lunula* could be used as a living flow biosensor in those experimental setups where traditional invasive instrumentation is not feasible.
This study also shows how fluid dynamics could be used to generate bioluminescent light patterns by proper tuning the fluid flow, as done in recent explorations[25–27]. While cellular stress was not assessed here, future investigations should evaluate the balance between light enhancement and biological viability. In this interdisciplinary perspective, hydrodynamics emerges as both a functional and design parameter, enabling the development of visually expressive systems where light emission is shaped by the flow.

Methodology

Experimental apparatus

The experiment is conducted using living bioluminescent dinoflagellate of the species *Pyrocystis lunula*, whose microscope photograph is shown in Figure 4. The organisms, along with algal nutrients, are purchased from the company BioGlow Bioluminescence[28] and subsequently cultivated at MaBa.SaperLab[29], Politecnico di Milano. The initial concentration of the dinoflagellates at the time of purchase was approximately 30 cells/mL, which was already sufficient to allow bioluminescence to be observed. However, the experiments were conducted eight weeks after the sample arrived, when the algal population had increased to approximately 120 cells/ml.

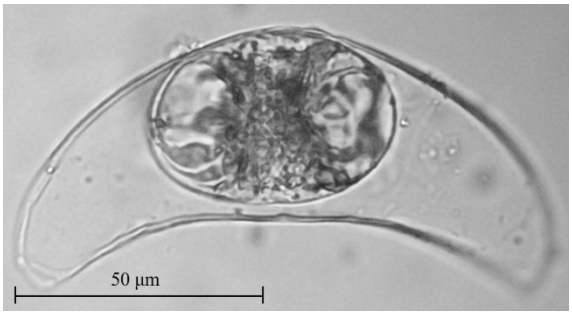

Figure 4: Microscope photograph of *Pyrocystis lunula*, the dinoflagellate species used in the present study as a tracer of vortex structures.

The experimental setup consists of a cylindrical glass container, HYCC MX-8K magnetic stirrer, and a full-spectrum LED lamp. The container has an internal diameter of 10,8 cm and is filled with dinoflagellate and seawater to reach a height of 13,8 cm.

The stirrer bar has a length of 0,03 m and a height of 0,008 m and has been placed at the center of the glass container. The lamp is a HALO GROW LIGHT (Model: BL-B20B; 1 HEAD; 80 LEDS), employed to invert the circadian rhythm of *Pyrocystis lunula* in order to perform experiments during daytime hours; the glass container is placed in a dark room under the lamp, which is programmed to turn on for 12 hours during the night, from 7:00 PM to 7:00 AM. With this light/dark cycle inversion, *Pyrocystis lunula* receives light at night and emit bioluminescence during the day. All experiments are carried out at a laboratory temperature range between 20 °C - 25 °C, with seawater pH of 6,41.

Bioluminescence imaging acquisition is performed using a Canon EOS 5D Mark III with EF17-40mm f/4L USM lens model, configured with f/4 aperture, 3200 ISO setting and with an exposure time of 30 seconds. For each angular velocity tested, three long-exposure photographs were taken, and the image with the best quality was selected for analysis. The angular velocity of the magnetic stirrer ranged between 152 rad/s and 160 rad/s: this is selected so that, using the Rankine (1858)[19] vortex model and Lautrup (2005)[21] formulation, the predicted shear stress threshold for the activation of *Pyrocystis lunula* bioluminescence can be reached on the vortex structure.

The experimental phase relates to the circadian rhythm of *Pyrocystis lunula* and its biological nature. Measurements were conducted in complete darkness, as bioluminescence is not detectable under illuminated conditions. Bioluminescence was not detectable during the initial hour of darkness, but became apparent roughly one hour after the onset of the dark phase. Additionally, a decrease in light intensity was observed as the light phase approached. Maximum light emission occurred qualitatively around the midpoint of the dark phase, neither too close to its beginning nor to the transition to the light phase. For this reason, the photographs were taken approximately five hours after the onset of the dark phase. Furthermore, the intensity of bioluminescence appears to decrease following prolonged exposure of *Pyrocystis lunula* to agitation, likely due to a temporary decrease in energy sources. To allow the cells to recharge, the dinoflagellates were left undisturbed in the dark for ten minutes between each photograph acquisition. Picture acquisition is made around one minute after the funnel formation, allowing for vortex geometry stabilization and a higher quality of the images. Each photograph is processed for vortex geometry data acquisition.

Geometry of a vortex induced by a magnetic stirrer

The reference used to evaluate the vortex depth and radius in swirling structures generated by a magnetic stirrer is the study conducted by Halasz et al. (2007)[18]. According to this work, the dimensions of the stirrer bar are key parameters in defining vortex shape - specifically a [m], the half-length of the bar, and d [m], the height of the bar. Two additional parameters contribute to the funnel geometry: the radius of the cylindrical container R [m], and the height of the resting fluid H [m]. Figure 5 illustrates the parameters used in the models and measured during the experimental study. The expressions used to estimate the funnel depth Δh [m] and half-width b [m] are[18]:

$$\Delta h = \frac{\Omega^2 \bullet a^2 \bullet d^2 \bullet R^{1/2}}{\nu \bullet (\alpha \bullet H + \kappa \bullet R) \bullet g^{1/2}} \quad (1) \qquad b = \frac{\beta \bullet a \bullet \nu}{d \bullet (g \bullet R)^{1/2}} \quad (2)$$

Where Ω is the angular velocity [rad/s], g is gravitational acceleration [m/s^2], and ν is the kinematic viscosity of the fluid [m^2/s]. α and κ are dimensionless parameters related to the function (H/R), while β is a dimensionless parameter related to the function (a/d). In the reference study, $\alpha = 580 \pm 80$, $\kappa = 2800 \pm 200$, $\beta = 2800 \pm 800$. As shown

in the model, knowing the geometry of both the stirrer bar and the cylindrical container along with the angular velocity and fluid properties, makes it possible to predict the vortex geometry. The results obtained from these expressions are compared to those derived experimentally. The kinematic viscosity of seawater is assumed to be $10{,}5 \cdot 10^{7} m^2/s$, based on a salinity of 35 g/kg and a temperature of 20 °C [30,31]. The funnel depth Δh [m] and half-width b [m] are compared to the ones measured from the photographs. The values of the parameters α, κ and β are calibrated to match the experimentally observed funnel depth and halfwidth.

Rankine vortex flow field

According to Rankine (1858)[19] "A combined vortex consists of a free vortex without and a forced vortex within a given cylindrical surface". The free vortex corresponds to the condition towards which any vortex tends in the absence of external forces, characterized by a velocity inversely proportional to the distance from the axis of rotation. In contrast, a forced vortex follows a different law, where the velocity increases with distance from the axis of rotation at a constant angular velocity, as if the fluid behaved like a rigid rotating body. In a combined vortex, both free and forced vortices coexist: at the junction point, the velocity and the free surface elevation must be equal, and the maximum depth of the free surface is twice that observed at the junction interface, as outlined by Rankine (1858)[19] in Fig. 251, page 577. In a combined vortex, a cusp appears in the velocity profile, resulting in a discontinuity in the shear stress that vanishes within the forced vortex region, highlighting that the Rankine (1858)[19] vortex is only valid in the case of an inviscid fluid[21]. It is possible to construct models that describe the tangential velocity profile using a single smooth interpolating function, which matches the Rankine (1858)[19] vortex in the limits $r \ll c$ and $r \gg c$, and ensures continuity in the shear stress profile[21]—e.g., the Lamb (1895)[32] vortex. The Burgers (1948)[23] vortex also represents a velocity field that maintains the interpolating tangential velocity profile of the Lamb (1895)[32] vortex, while additionally incorporating radial and axial velocity components[21].

In the present study, the formulation of tangential velocity and shear stress from the Rankine (1858)[19] vortex is adopted, in order to assess the validity of the model in predicting the shear stress field. The depth of the central depression can be estimated from bathtub-like vortex with circulation C [m^2/s][21]. Results are compared with those from the experiments and the empirical expressions from Halasz et al. (2007)[18]. The aim of the comparison is to match the predicted vortex geometries with the experimental ones, thereby relating the funnel shape to velocity and shear stress flow fields. According to the Rankine (1858)[19] vortex, the radial and the axial component of velocity are zero, and the only non-zero velocity component of the flow is tangential velocity v_ϕ[m/s], which exhibits a discontinuity at the core radius c [m][21]. The vortex profile h [m] and its associated parameters are shown in Figure 5:

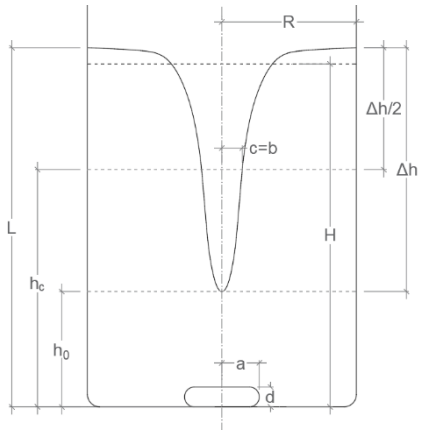

Figure 5: Cylindrical container, vortex structure and stirrer bar representation: geometrical parameters from Halasz et al. (2007)[18] on the right-side, bathtub-like vortex geometrical parameter from Lautrup (2005)[21] on the left-side, redrawn by Lucia Castellani. The value b from Halasz et al. (2007)[18] is set equal to the value c from Lautrup (2005)[21].

Vortex geometry can be obtained by matching the following expressions[21]:

$$c = \sqrt{\frac{C}{\Omega}} \quad (3) \qquad L - h_0 \approx \frac{C^2}{g_0 \bullet c^2} \quad (4) \qquad h_c \approx \frac{L + h_0}{2} \quad (5) \qquad h$$

$$\approx \begin{cases} h_0 + \dfrac{\Omega^2 \bullet r^2}{2 \bullet g_0} & r \ll c \\ L - \dfrac{C^2}{2 \bullet g_0 \bullet r^2} & r \gg c \end{cases} \quad (6)$$

$L - h_0$ [m] is the vortex depression depth, with h_0 [m] being the central height measured from the bottom for $r = 0$, $z = 0$, L [m] is the maximum height of the free surface and h_c [m] is the height at the core radius. The height of L [m] is measured from the photographs.

The shear stress $\tau_{\phi r}$[N/m^2] results from tangential velocity and acts in the radial direction. The flow field of a Rankine (1858)[19] vortex is described as follows[19,21]:

$$v_\phi = \begin{cases} \Omega \bullet r & 0 \le r \le c \\ \dfrac{\Omega \bullet c^2}{r} & c \le r \le \infty \end{cases} \quad (7) \qquad \tau_{\phi r} = \begin{cases} 0 & r < c \\ \dfrac{-2 \bullet \eta \bullet \Omega \bullet c^2}{r^2} & r > c \end{cases} \quad (8)$$

For r = c, the velocity formula for regions above the core is used, as it is slightly higher. The shear stress is also evaluated up to r = c, where η is seawater dynamic viscosity, assumed to be $1{,}077 \bullet 10^3$ kg/(m·s), based on a salinity of 35 g/kg and a temperature of 20 °C [30,31].

In this phase, experimental data are overlapped with the predicted ones. By assuming that the half-with b [m] from Halasz et al. (2007)[18] corresponds to the core radius c [m] from Lautrup (2005)[21], the vortex circulation C [m^2/s] is estimated from (3). The heights h_0 [m] and h_c [m] are calculated from (4) and (5), and the vortex profile h [m] is evaluated for every radial position $r \ll c$ [m] and $r \gg c$ [m] (6). The distance $L - h_0$ [m] is compared with Δh [m] and the funnel depth measured from the photographs. Lastly, the tangential velocity and shear stress fields are evaluated as functions of the radius, based on equations (7) and (8). For each angular velocity, the maximum shear stress value is identified and correlated with bioluminescence patterns observed in the vortex geometry photographs.

References

1. Schramm, S. & Weiß, D. Bioluminescence – The Vibrant Glow of Nature and its Chemical Mechanisms. *ChemBioChem* **25,** e202400106 (2024).
2. Shimomura, O. *Bioluminescence*. (WORLD SCIENTIFIC, 2006). doi:10.1142/6102
3. Martini, S. & Haddock, S. H. D. Quantification of bioluminescence from the surface to the deep sea demonstrates its predominance as an ecological trait. *Scientific Reports* **7,** 45750 (2017).
4. Haddock, S. H. D., Moline, M. A. & Case, J. F. Bioluminescence in the Sea. *Annual Review of Marine Science* **2,** 443–493 (2010).
5. Latz, M. I., Case, J. F. & Gran, R. L. Excitation of bioluminescence by laminar fluid shear associated with simple Couette flow. *Limnology and Oceanography* **39,** 1424–1439 (1994).
6. Rohr, J., Allen, J., Losee, J. & Latz, M. I. The use of bioluminescence as a flow diagnostic. *Physics Letters A* **228,** 408–416 (1997).
7. Latz, M. & Rohr, J. Luminescent response of the red tide dinoflagellate Lingulodinium polyedrum laminar and turbulent flow. *Limnology and Oceanography - LIMNOL OCEANOGR* **44,** 1423–1435 (1999).
8. Latz, M. Bioluminescence response of four species of dinoflagellates to fully developed pipe flow. *Journal of Plankton Research - J PLANKTON RES* **26,** 1529–1546 (2004).
9. Maldonado, E. & Latz, M. Shear-Stress Dependence of Dinoflagellate Bioluminescence. *The Biological bulletin* **212,** 242–9 (2007).
10. J. Rohr, M. I. Latz, E. Hendricks, & J. C. Nauen. A novel flow visualization technique using bioluminescent marine plankton II. Field studies. *IEEE Journal of Oceanic Engineering* **20,** 147–149 (1995).
11. Latz, M. I., Juhl, A. R., Ahmed, A. M., Elghobashi, S. E. & Rohr, J. Hydrodynamic stimulation of dinoflagellate bioluminescence: a computational and experimental study. *Journal of Experimental Biology* **207,** 1941–1951 (2004).
12. Letendre, F., Twardowski, M., Blackburn, A., Poulin, C. & Latz, M. A review of mechanically stimulated bioluminescence of marine plankton and its applications. *Frontiers in Marine Science* **10,** (2024).
13. Latz, M. & Lee, A. Spontaneous and stimulated bioluminescence of the dinoflagellate Ceratocorys horrida (Peridiniales). *Journal of Phycology* **31,** 120–132 (2008).
14. Deane, G. B., Stokes, M. D. & Latz, M. I. Bubble stimulation efficiency of dinoflagellate bioluminescence. *Luminescence* **31,** 270–280 (2016).
15. Blaser, S., Kurisu, F., Satoh, H. & Mino, T. Hydromechanical stimulation of bioluminescent plankton. *Luminescence : the journal of biological and chemical luminescence* **17,** 370–80 (2002).
16. Chen, A., Latz, M. & Frangos, J. The use of dinoflagellate bioluminescence to characterize cell stimulation in bioreactors. *Biotechnology and bioengineering* **83,** 93–103 (2003).
17. Einstein, A. Die Ursache der Mäanderbildung der Flußläufe und des sogenannten Baerschen Gesetzes. *Naturwissenschaften* **14(11),** 223–224 (1926).
18. Halasz, G., Gyure, B., Jánosi, I., Szabo, G. & Tel, T. Vortex flow generated by a magnetic stirrer. *American Journal of Physics* **75,** (2007).
19. Rankine, W. J. M. *A manual of applied mechanics*. (Richard Griffin and Company, 1858).
20. Knauss, J. *Swirling Flow Problems at Intakes*. (1987).
21. Lautrup, B. *Physics of Continuous Matter: Exotic and Everyday Phenomena in the Macroscopic World*. (2005).
22. Cussatlegras, A.-S. & Le Gal, P. Variability in the bioluminescence response of the dinoflagellate Pyrocystis lunula. *Journal of Experimental Marine Biology and Ecology* **343,** 74–81 (2007).
23. Burgers, J. M. in *Advances in Applied Mechanics* (eds Von Mises, R. & Von Kármán, T.) **1,** 171–199 (Elsevier, 1948).

24. Duinmeijer, A., Oldenziel, G. & Clemens, F. Experimental study on the 3D-flow field of a free-surface vortex using stereo PIV. *Journal of Hydraulic Research* **58,** 105–119 (2020).
25. GLOWING NATURE. at <https://www.studioroosegaarde.net/project/glowing-nature>
26. Latz, M. The artistry of dinoflagellate bioluminescence. *Materials Today: Proceedings* **4,** (2017).
27. Latz, M. The Making of Infinity Cube, a Bioluminescence Art Exhibit. *Limnology and Oceanography Bulletin* **28,** (2019).
28. BioGlow Bioluminescence: Webstore for bioluminescent algae. at <https://bioglow.eu/shop/en/>
29. MaBa.SAPERLab – Dipartimento ABC. at <https://www.dabc.polimi.it/abclab/le-unita/mabasaperlab/>
30. Nayar, K., Sharqawy, M., Banchik, L. & V, J. Thermophysical properties of seawater: A review and new correlations that include pressure dependence. *Desalination* **390,** 1–24 (2016).
31. Sharqawy, M. H., Lienhard, J. H. & Zubair, S. M. Thermophysical properties of seawater: a review of existing correlations and data. *Desalination and Water Treatment* **16,** 354–380 (2010).
32. Lamb, H. *Hydrodynamics*. (Cambridge University Press, 1895).

Aknowledgements
The authors gratefully acknowledge Saverio Pasquale Spadafora for the technical assistance throughout the entire experimental phase at MaBa.SAPERLab.
The works have been supported by the Grant PNRR-CN-AGRITECH-S3.

Author contributions
L.C.: Concept and design of the work – Acquisition, analysis and interpretation of data – Original draft writing. G.R.: Concept and design of the work – Acquisition, analysis and interpretation of data – Reviewing and editing. G.P.: Concept and design of the work – Analysis and interpretation of data – Reviewing and editing. S.G.: Acquisition, analysis and interpretation of data – Reviewing and editing. I.M.P.: Concept and design of the work – Reviewing and editing. M.M.: Concept and design of the work – Analysis and interpretation of data – Reviewing and editing. All authors reviewed the manuscript.

Data availability statement
The datasets generated and analysed during the current study are available from the corresponding author on reasonable request.

Competing interests
The authors declare no competing interests.